Probabilistic Tomography Maps Chemical Heterogeneities Throughout the Lower Mantle

Jeannot Trampert, Frédéric Deschamps, Joseph Resovsky, Dave Yuen

Materials and Methods

Density modeling

In a pioneering study, Ishii and Tromp (*S1*) showed that it was possible to obtain density models from normal mode data. The nature of the inverse problem, however, is such that the density part is heavily dependent on the employed regularization. This led to criticism of their study (*S2*-*S4*), but an extended data set and a new approach (*S5*), referred to as probabilistic tomography, can unambiguously isolate the density signal in the long period seismic data. We realized that the normal mode data used in (*S1*) suffered from trade-offs between upper and lower mantle signals, which could easily be broken by adding existing high quality fundamental mode and overtone surface wave data (*S6*). The probabilistic approach established that individual models are not necessarily meaningful, but the whole family of models (represented by a joint probability density function (pdf)), compatible with the data, has well defined properties (*S6*). Likelihoods of individual seismic parameters are found by marginalizing the joint pdfs obtained from a full model space search. These likelihoods contain no explicit regularization and are not biased by a chosen parameterization. They can thus be seen as a complete representation of the seismological constraints. We confirm that the probability p of a positive correlation between $d\ln\rho$ and $d\ln V_s$ is small ($p = 0.02$), and that the commonly used scalings between the two quantities are not justified ($p[0 < d\ln\rho/d\ln V_s < 0.5] = 0.08$). Using a similar data set to ours,

Ishii and Tromp (*S7*) obtained a density model which is close to ours in pattern in the lowermost mantle. Their amplitude is half of that of our most likely model and is a consequence of the damping which they have to prescribe.

Gravity filtering

The gravity field can be obtained by a simple static calculation (*S1*), independent of uncertain viscosity profiles, provided we have compatible information on density and topography. In the joint pdfs, an individual realization is a single compatible density-topography-velocity model fitting the seismic data. We drew randomly in these joint pdfs and calculated the corresponding non-hydrostatic gravity potential without crust and surface topography. We only kept those compatible models fitting the observed gravity potential within its error bars. These errors are dominated by the uncertainty of removing a crustal model including surface topography (*S5*). The posterior filtering has the advantage of identifying inconsistencies between seismic and gravity inferences on density rather than concealing them by merging the two for a joint inversion. Only a few extreme (low probability) models are eliminated, and modest changes (mainly narrowing of the likelihoods) occur in the density model distribution. The correlation between the most likely density models before and after gravity filtering varies between 0.60 and 0.67 depending on depth and the root-mean square (rms) amplitudes increase in the lowermost mantle while they decrease elsewhere. The most likely velocity models are hardly affected by this filtering (correlations vary between 0.90 and 0.98 and approximately no change in rms amplitudes). Which effect our models will have on inferences of viscosity, and how well they will explain other geodynamic data, remains to be tested using dynamic modeling. Current scaled density models together with published boundary topographies certainly give a significantly worse fit ($\chi^2/N > 3$) to our dataset than the models presented here ($\chi^2/N < 2$).

Correlation between seismic likelihoods

The width of the likelihoods of correlation serve as a reminder that interpreting a single tomographic model can be misleading, whereas the whole family of models compatible with the data, can present useful properties. For instance, the likelihood of correlation between bulk sound and shear wave speed (example shown in *S5*) in the lower 1000 km of the mantle is sufficiently wide to incorporate those of all recent tomographic models (reviewed in *S8*). This suggests that much of the debate on the cause of tomographic images (chemical for a negative correlation, thermal for a positive correlation) is generated by different ways of solving the inverse problem rather than by data constraints. Our integrated likelihood has a probability of 0.95 for a negative correlation, and hence a very likely chemical origin.

Mineral physics modeling

The lower mantle is assumed to be a mixture of (Mg,Fe,Ca)perovskite and magnesiowüstite. Aluminum content could be important, but published mineral physics data are not in sufficient agreement to calculate the effect (*S9*). Even very recent measuring attempts remain inconclusive (*S10-S12*) so that we chose to neglect aluminum. To calculate density and all elastic moduli at high temperature and pressure, we used the method of Trampert et al. (*S13*). The equation-of-state modeling has been extended to accommodate the simultaneous use of experimental and ab initio data. There seems to be an inconsistently in the shear data, and a cross-derivative has been introduced at zero pressure to ensure compatibility of all data (*S9*). The iron dependence is introduced at the individual mineral level by corrections to the magnesium end-member at ambient conditions. Iron is shared between perovskite and magnesiowüstite via a partitioning coefficient. Calcium is modeled in a similar way, but Ca enters perovskite only. The mineral physics data used to calculate the sensitivities of seismic parameters to thermo-chemical parameters are shown in Table S1. The sensitivities have some dependence on the assumed reference

state. We therefore do not fix a reference state, but vary all parameters within reasonable ranges (*S13*) for the lower mantle. The total iron content is varied between 5 and 15 %, the iron partitioning between 0.2 and 0.5. Calcium content changes between 0 and 12 %. The foot of the adiabat is taken between 1500 and 2500 K, and the total perovskite content in the lower mantle is assumed to be between 50 and 100 %. These ranges together with uncertainties in the input parameters (Tab. S1) allow to generate many seismic profiles. Only those compatible with a seismic reference model are retained (*S13, S9*). For all profiles fitting the seismic reference model, we calculate the sensitivities by straightforward numerical differentiation (*S13, S9*). We then average the sensitivities and determine their standard deviation. This is a natural way to assess uncertainties in sensitivities simultaneously due to our ignorance of the Earth's thermo-chemical reference state and uncertainties in mineral physics data. Partial derivatives for many different parameters may be calculated. We retain only those which are large for at least one of the seismic parameters $d\ln V_s$, $d\ln V_\Phi$ or $d\ln\rho$ (Fig. S1). This leaves us with sensitivities for the total perovskite content. Note that its uncertainty reflects the fact that it may contain iron and calcium, but not aluminum. The other significant sensitivity is for the total iron content. Part of its uncertainty comes from our ignorance on how exactly iron is partitioned between perovskite and magnesiowüstite. Calcium variations induce small variations on all seismic parameters and hence cannot reliably be resolved. Given existing error bars on seismic parameters and sensitivities, neglecting calcium will probably not bias the results. Some partial derivatives are different from Deschamps and Trampert (*S14*) due to the fact that we included the latest published data for iron content in perovskite (*S15*) and magnesiowüstite (*S16*). Indeed, shear wave sensitivities to iron and perovskite depend on the assumed effect of iron at zero temperature and pressure (*S9*). We tested that this only slightly affects amplitudes of the inferred thermo-chemical variations, but not their sign and location.

Correlation between seismic and thermo-chemical parameters

In most interpretations of tomography, it is assumed that wave speeds, and in particular shear wave speeds, can be scaled to temperature. We have independent estimates (with almost no observed covariance) of likelihoods for $d\ln V_s$, $d\ln V_\Phi$ and $d\ln\rho$. System (1-3) is a perfectly determined problem and hence the pdfs for the thermo-chemical parameters dT, dPv or dFe are independent as well. We can thus calculate the likelihoods of correlation between any of these parameters. In our lowermost layer (`Fig. S2`), the correlation between $d\ln V_s$ and dT is indeed very low and shear wave speeds correlate much better with iron or perovskite variations. Temperature cannot be obtained by scaling shear wave speed, but is to a large extend determined by density. Although the correlation between $d\ln V_s$ and dT improves higher in the mantle, it never exceeds 0.7 in absolute value for a given pair drawn in the Gaussian distributions of the models. Notable very high correlations throughout the mantle (only shown for our lowermost layer) are between $d\ln V_\Phi$ and dPv, and between $d\ln\rho$ and dFe.

References

S1 M. Ishii, J. Tromp, *Science* **285**, 1231 (1999).

S2 J. S. Resovsky, M. H. Ritzwoller, *Geophys. Res. Lett.* **26**, 2319 (1999).

S3 B. Romanowicz, *Geophys. Res. Lett.* **28**, 1107 (2001).

S4 C. Kuo, B. Romanowicz, *Geophys. J. Int.* **150**, 162 (2002).

S5 J. Resovsky, J. Trampert, *Earth Planet. Sci. Lett.* **215**, 121 (2003).

S6 J. S. Resovsky, J. Trampert, *Geophys. J. Int.* **150**, 665 (2002).

S7 M. Ishii, J. Tromp, *Phys. Earth Planet. Int.* **146**, 113 (2004).

S8 G. Masters, G. Laske, H. Bolton, A. M. Dziewonski, in *Earth's Deep Interior: mineral Physics and Tomography From the Atomic to the Global Scale*, S.-I.

Karato et al., Eds. (American Geophysical Union, Washington, DC, 2000) pp. 66-87.

S9 F. Deschamps, J. Trampert, *Earth Planet. Sci. Lett.* **222**, 161 (2004).

S10 I. Daniel, J. D. Bass, G. Fiquet, H. Carden. J. Zhang, M. Hanfland, *Geophys. Res. Lett.* **31**, doi: 10.1029/2004GL020213 (2004).

S11 J.M. Jackson, J. Zhang, J.D. Bass, *Geophys. Res. Lett.* **31**, doi: 10.1029/2004GL019918 (2004).

S12 T. Yagi, K. Okabe, N. Nishiyama, A. Kubo, T. Kikegawa, *Phys. Earth Planet. Inter.* **81**, 143 (2004).

S13 J. Trampert, P. Vacher, N. Vlaar, *Phys. Earth Planet. Int.* **124**, 255 (2001).

S14 F. Deschamps, J. Trampert, *Phys. Earth Planet. Int.* **140**, 277 (2003).

S15 B. Kiefer, L. Stixrude, R. M. Wentzcovitch, *Geophs. Res. Lett.* **29** doi:10.1029/2002GL014683 (2002).

S16 J. Kung, B. Li, D. J. Weidner, J. Zhang, R. C. Liebermann, *Earth Planet. Sci. Lett.* **203**, 557 (2002).

S17 A.R. Oganov, J.P. Brodholt, G.D. Price, *Earth Planet. Sci. Lett.* **184**, 555 (2001).

S18 Y. Wang, D.J. Weidner, F. Guyot, *J. Geophys. Res.* **101**, 661 (1996)

S19 B.B. Karki, J. Crain, *Geophys. Res. Lett.* **25**, 2741 (1998).

S20 S.V. Sinogeikin, J.D. Bass, *Phys. Res.* **B59**, 14141 (1999).

S21 B.B. Karki, R. M. Wentzcovitch, S. de Gironcoli, S. Baroni, *Phys. Res.* **B61**, 8793 (2000).

S22 Y. Sumino, O.L. Anderson, I. Suzuki, *Phys. Chem. Miner.* **9**, 38 (1983).

	perovskite (pv)			magneiowüstite (mw)	
	$MgSiO_3$	C_{Fe}^{pv}	C_{Ca}^{pv}	MgO	C_{Fe}^{mw}
ρ (g/cm3)	4.109	1.03 (*S15*)	0.122 (*S18*)	3.584	2.28
K_{S0} (GPa)	264.0	20.0 (*S15*)	-30.2 (*S18*)	162.5	18.0 (*S16*)
K'_{S0}	3.97/3.95/3.77/3.75	0.16 (*S15*)	0.73 (*S18*)	4.0 (*S20*) to 4.15 (*S21*)	-0.53 (*S16*)
$\dot{K}_{S0}$ (10^{-2} GPa/K)	-1.1/-1.5/-1.0/-1.5		-0.014 (*S18*)	-1.55 (*S22*) to -1.4 (*S21*)	
G_0 (GPa)	180.0 (*S17*)	-40.0 (*S15*)	-10.0 (*S19*)	130.8	-108.0 (*S16*)
G'_0	1.5 [0.05] (*S17*)	-0.52 (*S15*)	0.66 (*S19*)	2.4 (*S20*) to 2.5	-3.29 (*S16*)
$\dot{G}_0$ (10^{-2} GPa/K)	-2.0 [0.08] (*S17*)			-2.4 to -2.2 (*S21*)	
γ_0	1.31/1.39/1.33/1.41			1.41	
q	1.0/2.0/1.0/2.0			1.3	
a_1 ($10^{-5}K^{-1}$)	1.19 [0.17]			3.681	
a_2 ($10^{-8}K^{-2}$)	1.20 [0.10]			0.9283	
a_3 (K)	0.0			0.7445	

Table S1: All data are from Trampert et al. (*S13*), unless otherwise stated. When available, error bars are indicated in square brackets. ρ is the density, K_{S0} the abibatic bulk modulus, G_0 the shear modulus and γ_0 the Grüneisen parameter at ambient temperature and pressure. q is a constant. Primes and dots denote derivation with respect to pressure and temperature, respectively. Thermal expansitvity at zero pressure is given by $\alpha = a_1 + a_2 T - a_3 T^{-2}$. Where available, parameters are corrected for iron and calcium content X using $M = M_{Mg} + C_{Fe} X_{Fe} + C_{Ca} X_{Ca}$.

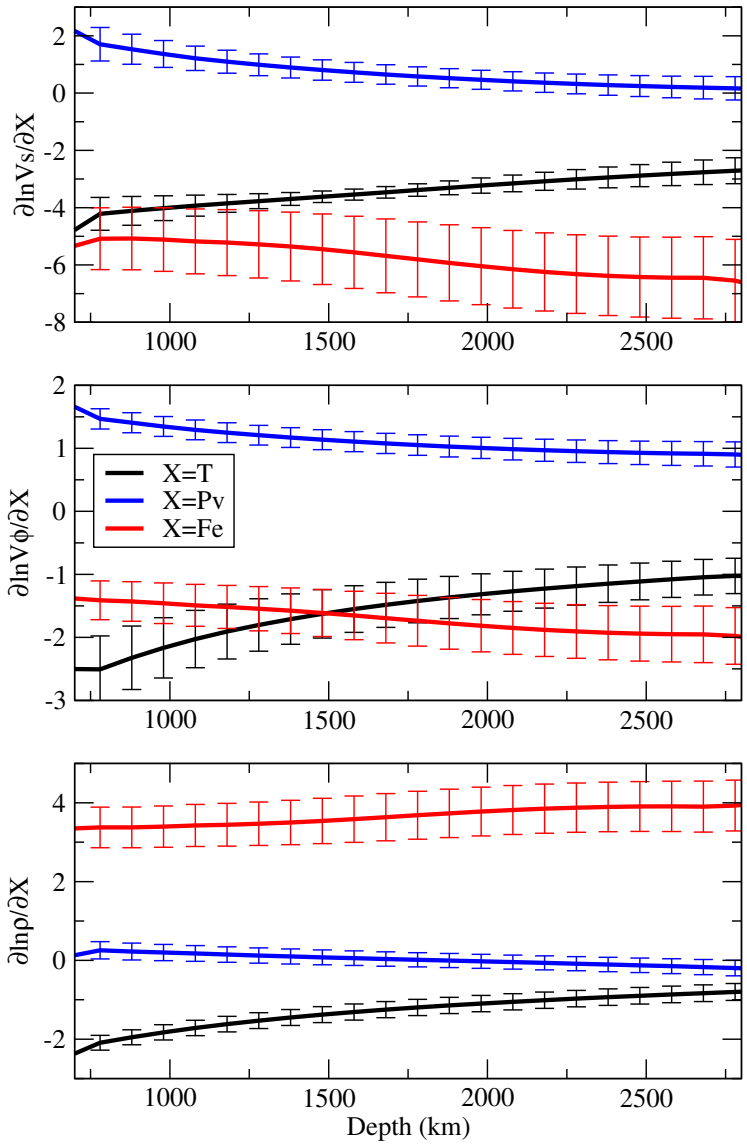

Figure S1: Sensitivities used in this study. Shown is the mean and standard deviation. For display only, the temperature derivatives are pre-multiplied by 10^5 all other derivatives by a factor of 10. Thermal expansivity $-\alpha = \partial \ln \rho / \partial T$ is seen on the black curve of the bottom panel.

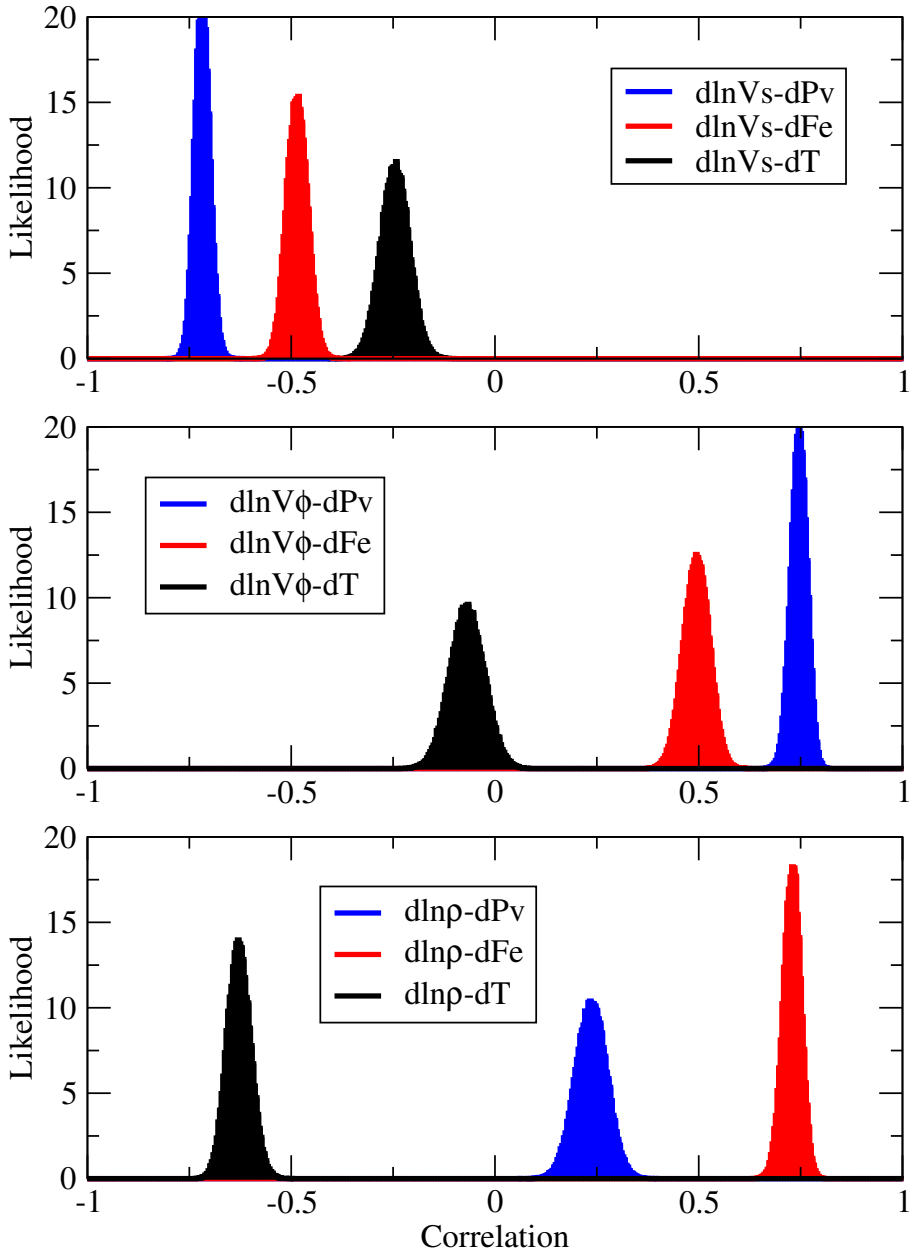

Figure S2: Likelihoods for correlations in the lowermost mantle layer [2000-2891 km].